Published in final edited form as:
Cell. 2013 November 7; 155(4): 778–792. doi:10.1016/j.cell.2013.09.059.

Lin28 enhances tissue repair by reprogramming cellular metabolism

Ng Shyh-Chang[1,2,3,4,5,6,10,#], **Hao Zhu**[1,2,3,4,5,7,8,10], **T. Yvanka de Soysa**[1,2,3,4,5], **Gen Shinoda**[1,2,3,4,5], **Marc T. Seligson**[1,2,3,4,5], **Kaloyan M. Tsanov**[1,2,3,4,5], **Liem Nguyen**[8], **John M. Asara**[6], **Lewis C. Cantley**[6,9], and **George Q. Daley**[1,2,3,4,5,*]

[1]Stem Cell Transplantation Program, Division of Pediatric Hematology/Oncology, Boston Children's Hospital and Dana Farber Cancer Institute, Boston, MA 02115, USA

[2]Department of Biological Chemistry and Molecular Pharmacology, Harvard Medical School, Boston, MA 02115, USA

[3]Harvard Stem Cell Institute, Boston, MA 02115, USA

[4]Manton Center for Orphan Disease Research, Boston, MA 02115, USA

[5]Howard Hughes Medical Institute, Boston, MA 02115, USA

[6]Department of Medicine, Division of Signal Transduction, Beth Israel Deaconess Medical Center, Boston, MA 02115, USA

[7]Division of Medical Oncology, Dana Farber Cancer Institute, Boston, MA 02115, USA

[8]Children's Research Institute, Departments of Pediatrics and Internal Medicine, University of Texas Southwestern Medical Center, Dallas, TX 75390, USA

[9]Department of Medicine, Cornell Weill Medical College, New York, NY 10065, USA

SUMMARY

Regeneration capacity declines with age, but why juvenile organisms show enhanced tissue repair remains unexplained. *Lin28a*, a highly-conserved RNA binding protein expressed during embryogenesis, plays roles in development, pluripotency and metabolism. To determine if *Lin28a* might influence tissue repair in adults, we engineered the reactivation of *Lin28a* expression in several models of tissue injury. *Lin28a* reactivation improved hair regrowth by promoting anagen in hair follicles, and accelerated regrowth of cartilage, bone and mesenchyme after ear and digit injuries. *Lin28a* inhibits *let-7* microRNA biogenesis; however *let-7* repression was necessary but insufficient to enhance repair. *Lin28a* bound to and enhanced the translation of mRNAs for several metabolic enzymes, thereby increasing glycolysis and oxidative phosphorylation (OxPhos). *Lin28a*-mediated enhancement of tissue repair was negated by OxPhos inhibition, whereas a

[*]Correspondence: george.daley@childrens.harvard.edu.
[10]These authors contributed equally to this work.
[#]Current address: Genome Institute of Singapore, 60 Biopolis Street, Singapore 138672

AUTHOR CONTRIBUTIONS

N.S.C. and H.Z. designed and performed the experiments. N.S.C., H.Z., and G.Q.D. wrote the manuscript. G.S., T.Y.D., M.T.S., L.N., K.M.T. helped with various experiments and mouse husbandry. J.M.A. helped with metabolomics and L.C.C. supervised all metabolism experiments. G.Q.D. designed and supervised experiments, and wrote the manuscript.

pharmacologically-induced increase in OxPhos enhanced repair. Thus, *Lin28a* enhances tissue repair in some adult tissues by reprogramming cellular bioenergetics.

INTRODUCTION

Throughout the evolutionary spectrum of organisms, the juvenile state is associated with superior tissue repair (defined as the partial or complete restoration of cellular content and tissue integrity after injury). *Drosophila* and *Tribolium* larvae repair robustly, but the adult insects do not (Smith-Bolton et al., 2009; Shah et al., 2011). Tadpoles, but not adult frogs, can repair multiple tissues (Sánchez Alvarado and Tsonis, 2006), and in *Ambystoma* salamanders, regenerative capacity declines with age (Young et al., 1983). Young fish repair their caudal fins better than older ones (Anchelin et al., 2011), and it is well-known that during gestation, fetal mammals repair their tissues more robustly than older mammals (Deuchar, 1976; Conboy et al., 2005; Nishino et al., 2008; Porrello et al., 2011). In contrast, insects like the *Apterygota*, which do not undergo complete metamorphosis, retain remarkable larval capacities for appendage repair throughout life (Pearson, 1984), and some hyper-regenerative urodeles such as the neotenic Axolotl fail to undergo metamorphosis and exhibit larval regenerative potential throughout their lifespan. These exceptions notwithstanding, the correlation between juvenility and tissue repair has long been discussed by Charles Darwin and others (Darwin, 1887; Pearson, 1984; Poss, 2010), but the causal mechanisms remain obscure.

Lin28 is an RNA-binding protein first described in a *C. elegans* screen for heterochronic genes that regulate developmental timing. Loss of *lin-28* causes precocious larval progression to adulthood, whereas gain of *lin-28* delays larval progression and reiterates larval cell stages by promoting progenitor self-renewal (Ambros and Horvitz, 1984; Moss et al., 1997). Mammalian *Lin28* exists as two highly-conserved paralogs, *Lin28a* and *Lin28b*, both of which repress *let-7* microRNAs (Viswanathan et al., 2008; Newman et al., 2008; Heo et al., 2008; Rybak et al., 2008). In mammals, *Lin28a* is highly expressed in embryonic stem cells (ESCs) and during embryogenesis, whereas mature *let-7* rises as Lin28a levels wane during ESC differentiation, fetal development and aging (Shyh-Chang and Daley, 2013). *Lin28a* has also been used to reprogram human somatic cells into induced pluripotent stem (iPS) cells (Yu et al., 2007) and in mice, *Lin28a* overexpression delays puberty and promotes growth (Zhu et al., 2010, 2011). *Lin28b* is also expressed in ESCs and extinguished in most tissues after birth, but it is not yet known if there are different physiologic roles or molecular targets for *Lin28a* and *Lin28b*. Conditional reactivation of *Lin28a* and *LIN28B* in adult mice prevents obesity and type 2 diabetes during aging, whereas conditional loss of *Lin28a/b* in fetuses causes dwarfism and promotes a diabetic state (Zhu et al., 2011; Shinoda et al., 2013). The human *LIN28B* gene shows polymorphisms strongly associated with puberty and height, indicating that the influence of Lin28 on development is evolutionarily conserved from worms to humans (Lettre et al., 2008; Widén et al., 2010; Ong et al., 2009; Sulem et al., 2009; Perry et al., 2009; Ong et al., 2011; Leinonen et al., 2012).

Prior studies linking Lin28 to juvenile programs of growth, development and metabolism led us to ask if reprogramming the developmental age of tissues with Lin28 could influence their post-natal repair capacities. Here we report that engineering the re-expression of Lin28a can enhance tissue repair in several contexts. Surprisingly, *let-7* repression is necessary but alone insufficient to account for Lin28a's enhancement of tissue repair. Lin28a also binds and increases the translation of the mRNAs for several metabolic enzymes including *Pfkp, Pdha1, Idh3b, Sdha, Ndufb3* and *Ndufb8* which, as established through metabolomic profiling, enhance oxidative metabolism to promote an embryonic bioenergetic state. Pharmacologic studies with inhibitors show that *Lin28a*-mediated tissue repair is more

sensitive to OxPhos inhibition than is normal tissue repair. These data suggest that *Lin28a* promotes repair capacities in post-natal tissues by enhancing oxidative metabolism, both glycolysis and OxPhos, and promoting a bioenergetic state characteristic of embryonic cells.

RESULTS

Lin28a promotes epidermal hair regrowth

Lin28a is expressed in the embryonic epidermis, but disappears by birth (Yang and Moss, 2003). We previously described a doxycycline (dox)-inducible *Lin28a* transgenic mouse ("iLin28a Tg") with constitutive low levels of leaky *Lin28a* expression in the absence of induction (Zhu et al., 2010). Relative to non-transgenic wild type littermates (WT), iLin28a Tg mice displayed thicker hair coats and increased skin thickness (Fig. 1A and Fig. S1A), correlating with *Lin28a* overexpression and *let-7* repression in the epidermis (Fig. 1B–D). The hair appearance was not explained by greater hair follicle density or follicle bulb diameter (Fig. S1B,C). Given these observations, we asked if *Lin28a* overexpression might influence hair growth.

In mice, the hair follicle cycle is normally synchronized for the rst 10 weeks of life (Muller-Rover et al., 2001). The rst post-natal growth phase (anagen) ends at approximately post-natal day 16 (p16), followed by the rst resting phase (telogen). The second anagen begins at p28 and is followed by a second protracted telogen phase between p42 and p70 (Muller-Rover et al., 2001). We shaved the hair of mice expected to be in the first and second telogen phases (p21 and p70), and found that iLin28a Tg mice displayed enhanced dorsal hair regrowth at both of these time points (Fig. 1E). To explore the mechanism of this growth difference, we performed a full 10-week hair cycle survey and found that while WT mice conform to the expected timing of the anagen-telogen phases, iLin28a Tg mice have extended periods of anagen and shortened telogen (Fig. 1F). Specifically, WT mice were in telogen at p20, 24, 42, 47, 49, 56 and 69, while iLin28a Tg mice manifested only a brief resting phase at p42 and p47. We then asked if hair regrowth occurs differently in WT and iLin28a Tg mice when both are in anagen. We synchronized hair cycling using wax depilation, which removes the entire hair follicle and thus induces anagen in both genotypes, and found no differential in hair regrowth during anagen (Fig. S1D), which was corroborated by equivalent cell proliferation in anagen hair follicles (Fig. S1E). Additionally, we inquired if *Lin28a* induction could induce anagen during a telogen phase. We induced *Lin28a* by topical application of dox at p47, when both WT and iLin28a Tg mice were in telogen. Dox treated WT or DMSO treated iLin28a Tg mice showed no hair regrowth, whereas iLin28a Tg mice with topical dox showed patchy hair regrowth after 7 and 14 days, indicating that *Lin28a* overexpression during telogen is sufficient to induce anagen in hair follicles (Fig. 1G). Thus, *Lin28a* overexpression promotes hair regrowth by promoting anagen. Findings from this tissue context suggested that ectopic reactivation of *Lin28a* might be capable of promoting repair in other post-natal tissues as well.

Lin28a promotes digit repair

Lin28a mRNA is expressed in the embryonic limb buds of E9.5 – E11.5 embryos, but declines sharply by birth (Yokoyama et al., 2008). Limb digits consist of multiple tissue types and show limited repair capacity after amputation in neonatal mammals. To assess their repair, mouse digits were amputated at the distal interphalangeal joint on day 2 after birth, and digit length was measured at 3 weeks of age. Relative to WT neonates, iLin28a Tg neonates displayed significantly enhanced connective tissue and bone regrowth in amputated digit tips (Fig. 2A–C). Even after normalizing for the greater body growth in iLin28a Tg mice, *Lin28a* accelerated the regrowth of injured digits over time (Fig. 2D). Whereas *Lin28a* showed no significant increase in expression in WT digits following amputation, *Lin28a*

expression was elevated in iLin28a Tg digits before and after amputation (Fig. 2E–F). Consistent with this pattern, only *let-7b* dropped after digit amputation in WT mice, whereas several *let-7* species were repressed both before and after injury in iLin28a Tg mice (Fig. 2G).

We next asked if *Lin28a* overexpression could further improve tissue repair in MRL mice, a well-known hyper-regenerative strain (Clark et al., 1998; Chadwick et al., 2007; Gourevitch et al., 2009). After backcrossing iLin28a Tg mice onto the MRL strain for 5 generations, *Lin28a* overexpression further enhanced digit tip repair relative to WT MRL controls, suggesting non-overlapping, additive mechanisms of enhanced repair. This supports the idea that even the repair capacity of the MRL strain could be augmented by genetic reactivation of *Lin28a* (Fig. 2H).

Because *Lin28a* improved neonatal digit repair, we hypothesized that *Lin28a* overexpression might also improve adult digit tip repair. In 5-week old mice, we amputated hindlimb digit tips, but found that reactivation of *Lin28a* expression conferred no significant enhancement of repair (Fig. S2), suggesting that *Lin28a* alone is insufficient to enhance adult repair in this context.

Lin28a promotes pinnal tissue repair

We assayed repair in the adult pinnal tissues of the outer ear, another complex tissue consisting of epidermis, cartilage and mesenchyme that fails to regenerate completely upon injury (Goss and Grimes, 1975; McBrearty et al., 1998; Liu et al., 2011). Low-level leaky *Lin28a* overexpression in the iLin28a Tg mice enhanced wound healing after 2mm full-thickness punch biopsy (Fig. 3A), as indicated by smaller wound sizes detected at 5, 8, and 11 days (Fig. 3B). In WT mice, 28% of the wounds could not be evaluated quantitatively because of poor healing and severe tearing of the wounds, whereas only 2% of wounds in iLin28a Tg mice displayed such severe damage (Fig. 3C). Similar to the digits, we observed a transient drop in *let-7b* following injury (Fig. 4A), but did not observe an increase in *Lin28a* during WT tissue repair (Fig. 3D, E). To determine if direct activation of *Lin28a* at the site of injury would promote pinnal repair, we applied dox topically onto wounds after punch biopsy. We detected local induction of *Lin28a* protein (Fig. 3D) and mRNA (Fig. 3E), and measured 50% greater wound closure after 11 days relative to uninduced iLin28a Tg ears (Fig. 3F). *Hmga2*, a prominent *let-7* target, was also induced in iLin28a Tg but not in WT ears (Fig. 3E). Histologically, there was an increase in mesenchymal connective tissue after local *Lin28a* induction, and an increase in proliferation according to Ki67 staining (Fig. 3G), indicating that *Lin28a* induction promotes mesenchymal cell proliferation and tissue repair in pinnae. Interestingly, local dox induction of *LIN28B* in iLIN28B Tg mice (Zhu et al. 2011) was not sufficient to promote ear wound healing, suggesting a *Lin28a*-specific mechanism for this process (Fig. S3).

Repression of let-7 is necessary but insufficient for promoting tissue repair

A major downstream effect of *Lin28* is the repression of *let-7* microRNAs. Because a subset of *let-7* miRNAs decreased after digit and pinnal injury in WT animals (Fig. 2G, 4A), we hypothesized that repression of *let-7* might be essential to tissue repair, and that enforced expression of *let-7* would antagonize wound healing. We therefore assessed tissue repair in a transgenic mouse that expresses a dox-inducible form of the *let-7* miRNA (“iLet-7 mice”; Zhu et al. 2011). Indeed, enforced overexpression of *let-7* after ear punch biopsy inhibited wound closure and pinnal repair relative to uninduced mice, suggesting that *let-7* repression is necessary for tissue repair (Fig. 4B). To test if *let-7* repression would be sufficient to phenocopy the enhanced tissue repair observed with overexpression of *Lin28a*, we used a locked nucleic acid (LNA)-modified antimiR to antagonize *let-7* function. Previously, *let-7*

antimiRs successfully reduced mature *let-7* levels and promoted an anti-diabetic phenotype in mice, thus phenocopying *Lin28a* overexpression (Frost and Olson 2011; Zhu et al. 2011). In our experiments, the *let-7* antimiR repressed a wide range of mature *let-7*'s in MEFs and in vivo (Fig. 4C–E), to a greater extent than achieved by *Lin28a* overexpression. However, despite an efficient knockdown of *let-7*, neither systemic nor topical delivery of *let-7* antimiR enhanced pinnal tissue repair (Fig. 4F,G) nor hair regrowth (Fig. 4H). These data indicate that *let-7* antagonizes normal tissue repair, but also suggest that *let-7* repression is necessary but not alone sufficient to explain the mechanism of enhanced tissue repair by Lin28a.

Lin28a alters the bioenergetic state during tissue repair

Lin28a/b and *let-7* are known to regulate glucose metabolism, and transcripts encoding mitochondrial oxidative phosphorylation (OxPhos) and glycolysis enzymes are among the top mRNAs bound by *Lin28a* (Peng et al., 2011; Zhu et al., 2011). To test the metabolic role of *Lin28a* in its most physiologically relevant context, we profiled metabolism in whole *Lin28a*$^{-/-}$ *Lin28b*$^{-/-}$ embryos vs. *Lin28a*$^{+/+}$ *Lin28b*$^{-/-}$ embryos at E10.5 using Liquid Chromatography/Tandem Mass Spectrometry metabolomics (Shyh-Chang et al., 2013a). *Lin28a* deficiency led to lower levels of some glycolytic intermediates (Fig. S5A), lower ATP/AMP and NADH/NAD ratios, and higher levels of reduced glutathione (higher GSH/GSSG ratio, which indicates lower levels of reactive oxygen species or ROS; Fig. S5B). These data demonstrate that *Lin28a* is physiologically required for normal embryonic bioenergetics, and are consistent with our previous study that compared *Lin28a*$^{+/-}$ to *Lin28a*$^{-/-}$ embryos and likewise concluded that *Lin28a* is essential for normal embryonic metabolism (Shinoda et al., 2013).

These precedents prompted us to profile the metabolomic effects of *Lin28a* reactivation during tissue repair. We found that *Lin28a* induction led to an increase in several glycolytic intermediates in pinnal tissues after injury, suggesting a general increase in glucose oxidation, whereas WT ears exhibited few changes (Fig. 5A). *Lin28a* induction also enhanced the bioenergetic state during tissue repair in vivo, as indicated by the increase in acetyl-CoA, and the increased ATP/AMP and GTP/GMP bioenergetic ratios (Fig. 5B).

Using ^{13}C-glucose, we measured the flux of glucose through glycolysis and the Krebs cycle in MEFs, and found that *Lin28a* increased ^{13}C-glucose flux into glycolysis (Fig. 5C), as well as the Krebs cycle (Fig. 5D), consistent with our observations in vivo. Furthermore, we found that the ATP/AMP ratio increased whereas the GSH/GSSG ratio decreased significantly with *Lin28a* overexpression (Fig. 5E), confirming that *Lin28a* enhances glucose oxidation to produce more ATP and ROS during tissue repair.

To determine if *Lin28a* was promoting the bioenergetic state by simply increasing mitochondrial biogenesis, we measured mitochondrial markers. We failed to detect increases in the mRNA levels of mitochondrial biogenesis markers and enzymes (Fig. 5F); there was no change in mitochondrial DNA (Fig. S5C); and CMXRos staining revealed no significant changes in the mitochondrial density and distribution (Fig. S5D). These data indicate that *Lin28a* enhances mitochondrial OxPhos activity rather than mass. We confirmed this using the Seahorse analyzer to measure the O_2 consumption rates of primary MEFs from iLin28a Tg mice. Relative to WT control MEFs, *Lin28a* increased both the basal and maximal OxPhos capacity, as indicated by the increases in O_2 consumption (Fig. 5G). *Lin28a* also increased the basal glycolytic capacity (Fig. 5H), consistent with findings from ^{13}C-glucose flux studies.

To assess if *Lin28a* was causing metabolic changes in a *let-7*-dependent manner, we transfected a *let-7* mimic and/or the *let-7* antimiR into WT and iLin28a Tg MEFs. As

expected, the *let-7* LNA antimiR led to *let-7* repression (Fig. 5I) and increased expression of the canonical *let-7* targets *Hmga2* and *Imp2* (Fig. 5J), whereas the *let-7* mimic led to the converse (Fig. 5I–J). ^{13}C-glucose flux metabolomic profiling of these transfected MEFs then revealed that *let-7* repression phenocopied Lin28a's enhancement of glycolytic flux (into 3-phosphoglycerate and serine biosynthesis), whereas enforced *let-7* overexpression suppressed WT glycolysis and partially abrogated Lin28a's enhancement of glycolysis (Fig. 5K). However, *let-7* repression failed to fully phenocopy Lin28a's enhancement of Krebs cycle flux, and enforced *let-7* overexpression failed to reduce WT Krebs cycle flux, although it did partially abrogate Lin28a's enhancement of Krebs cycle flux (Fig. 5L). Most importantly, *let-7* repression failed to phenocopy Lin28a's enhancement of OxPhos, and enforced *let-7* overexpression failed to block Lin28a's enhancement of OxPhos (Fig. 5M). These results show that *let-7* perturbation only partially phenocopies the metabolic effects of Lin28a, and support our conclusion that *let-7* perturbation alone is necessary but insufficient to phenocopy Lin28a's effects on tissue repair.

Lin28a promotes the expression of oxidative enzymes

Although Lin28a is well-known as a repressor of *let-7* microRNA biogenesis, Lin28a also regulates mRNA translation independently of *let-7* (Polesskaya et al., 2007; Peng et al., 2011; Wilbert et al., 2012; Cho et al., 2012). To show that Lin28a directly binds metabolic enzyme mRNAs in primary MEFs and pinnal tissues, we used RNA immunoprecipitation (RIP) to show that FLAG-tagged Lin28a binds to mRNAs for *Pfkp, Pdha1, Idh3b, Sdha, Ndufb3* and *Ndufb8* (Fig. 6A,B). Furthermore, Lin28a overexpression resulted in increased protein levels of these metabolic genes, to varying degrees, in these settings (Fig. 6C), consistent with previous studies showing that Lin28a can directly enhance mRNA translation (Polesskaya et al., 2007). Interestingly, phosphofructokinase (Pfkp) and pyruvate dehydrogenase (Pdha1) are the rate-limiting enzymes that fuel glycolysis and the Krebs cycle respectively (Fig. S6A). Isocitrate dehydrogenase (Idh3b) is the mitochondrial enzyme that catalyzes the first oxidative decarboxylation step in the Krebs cycle to produce α-ketoglutarate, NADH and CO_2, whereas succinate dehydrogenase (Sdha) oxidizes succinate to produce fumarate and $FADH_2$, and also serves as Complex II in the electron transport chain. NADH dehydrogenases (Ndufb3/8) constitute the rate-limiting Complex I in the electron transport chain that oxidizes NADH for ATP synthesis during OxPhos. Hence, Lin28a directly binds and increases translation of multiple rate-limiting enzyme components in both glycolysis and OxPhos (Fig. 6A–C).

To determine if *Lin28a*-mediated metabolic enhancements might influence cell migration or proliferation, two processes that are critical for tissue repair (Guo and DiPietro, 2010), we subjected MEFs to in vitro migration and proliferation assays. Indeed, iLin28a Tg MEFs migrated more than WT MEFs (Fig. 6D). We then tested if pharmacological inhibition of glycolysis or OxPhos could influence MEF migration (see Fig. S6A for summary of inhibitor targets). OxPhos inhibition by antimycin-A, a specific electron transport chain Complex III inhibitor, reduced iLin28a Tg MEF migration more than WT MEFs (Fig. 6D). The glycolysis inhibitor 3-bromopyruvate (3BP) also reduced iLin28a Tg MEF migration more than WT MEFs (Fig. 6D), together suggesting that the enhanced cell migration associated with Lin28a expression is dependent upon enhanced glycolysis and OxPhos.

To determine if Lin28a influences cell migration in a *let-7*-dependent manner, we transfected the *let-7* LNA antimiR and *let-7* mimic into Tg and WT MEFs. *Let-7* repression had no significant effects on WT or iLin28a Tg MEF migration, whereas enforced *let-7* overexpression significantly inhibited both WT and iLin28a Tg MEF migration (Fig. 6E). These data are consistent with our observations that *let-7* repression alone is necessary but insufficient to recapitulate Lin28a's effects, suggesting that the mRNA targets of Lin28a

play critical roles. Indeed, siRNA knockdown of individual enzyme subunits like *Pfkp, Pdha1, Idh3b, Sdha, Ndufb3* or *Ndufb8* (Fig. S6A–E) all impaired cell migration for WT and Tg MEFs (Fig. 6F), indicating that the stoichiometries of these enzyme complexes are critical to cell migration.

Cell proliferation is critical for tissue repair as well, but the importance of OxPhos for this process is unclear. OxPhos inhibition by antimycin-A impaired the proliferation of both WT and iLin28a Tg MEFs (Fig. S6F) with no changes in apoptosis, suggesting that normal OxPhos is essential for cell proliferation. Overexpression of *let-7* inhibited cell proliferation in both WT and iLin28a Tg MEFs, whereas *let-7* repression did not significantly affect proliferation in either (Fig. 6G). These data are consistent with our observations that *let-7* repression is necessary but insufficient to recapitulate Lin28a's effects, suggesting that the mRNA targets of Lin28a are critical. Depletion of *Pfkp, Pdha1, Idh3b, Sdha, Ndufb3* or *Ndufb8* (Fig. S6A–E), led to a defect in cell proliferation for both WT and iLin28a Tg MEFs (Fig. 6H), showing that the stoichiometries of these enzyme complexes – regulated by Lin28a – are important for cell proliferation.

Over the course of long-term passaging, *Lin28a* suppressed MEF proliferation in vitro (Fig. S6F) while in vivo, *Lin28a* promoted cell proliferation in hair follicles (Fig. 1) and pinnal tissues (Fig. 3G). Lin28a is therefore likely to be inducing senescence in vitro after passaging, through oxidative stress (Miyauchi et al., 2004; Nogueira et al., 2008; Kaplon et al., 2013). This counterintuitive effect is also observed when other oncogenes like Kras, Braf and PI3K are over-expressed in cells cultured in vitro, even when these oncogenes are known to promote cell proliferation in vivo.

To assess the importance of *Lin28a*-mediated metabolic changes in vivo, we applied specific pharmacologic inhibitors of glycolysis and OxPhos in the setting of hair regrowth (Fig. 7A). As shown in Fig. 1, topical induction of Lin28a in the epidermis improves hair regrowth during telogen. OxPhos inhibition with topical antimycin-A (+dox) suppressed hair regrowth specifically in iLin28a Tg mice, with no effect on WT mice, indicating the effect was not due to overt tissue toxicity (Fig. 7A). Glycolysis inhibition with topical 3BP (+dox) also suppressed hair growth specifically in iLin28a Tg mice, without influencing WT mice. When the drugs were discontinued for 10 days, WT mice showed partial hair regrowth whereas iLin28a Tg mice showed complete regrowth, indicating that hair follicle cycling was only transiently, and not irreversibly inhibited by this dosing regimen (Fig. 7A). These results suggest that *Lin28a* promotes hair regrowth by enhancing glucose oxidation through both glycolysis and OxPhos.

We sought to confirm this mechanism in another tissue context. Hence, we blocked OxPhos by topically applying antimycin-A daily on ears following pinnal injury. Consistent with the results in hair regrowth, antimycin-A abrogated *Lin28a*'s enhancement of pinnal repair, with no significant effects on WT pinnae (Fig. 7B). This suggests that iLin28a Tg tissue repair is more sensitive to OxPhos inhibition than WT tissue repair. In contrast, the antioxidant N-acetyl-cysteine had only a small effect on pinnal repair in both WT and iLin28a Tg mice (Fig. 7C), thus excluding a role for ROS or ROS-induced macrophage recruitment in the *Lin28a* mechanism.

Surprisingly, daily topical application of glycolysis inhibitors (3BP or 2-deoxy-D-glucose (2DG)), induced a substantial enhancement in WT tissue repair, comparable to the *Lin28a*-mediated enhancement (Fig. 7D). 3BP also enhanced migration in WT MEFs (Fig. 6D). One possible result of glycolysis inhibition is a compensatory increase in OxPhos activity, a phenomenon observed in cancer cells (Wu et al. 2007). To test if a compensatory increase in OxPhos explains why glycolysis inhibition in WT ears enhances tissue repair similarly to

Lin28a overexpression (Fig. 7D), we performed metabolomic profiling on WT ears 1 and 7 days after daily 3BP treatment. 1 day after topical treatment, we found that 3BP drastically reduced glycolytic intermediates and decreased the NADH/NAD, ATP/AMP, ATP/ADP, and GTP/GMP bioenergetic ratios, as expected with glycolysis inhibition (Fig. 7E). After 7 days of daily 3BP treatment, however, the levels of glycolytic intermediates and the NADH/NAD ratio returned to normal, and there was a significant increase in the ATP/AMP and ATP/ADP ratios, indicating a compensatory increase in OxPhos activity in vivo (Fig. 7E). In WT MEFs, 3BP also led to an increase in ^{13}C-glucose flux through the Krebs cycle (Fig. 7F), and an increase in the maximal O_2 consumption rate (Fig. 7G), further confirming that chronic glycolysis inhibition by 3BP induces a compensatory increase in OxPhos to enhance tissue repair. Together with our results showing Lin28a's enhancement of OxPhos (Fig. 5A–M), and the necessity for increased OxPhos in Lin28a's enhancement of tissue repair in vivo (Fig. 7A–G), these results suggest that an enhancement of oxidative metabolism by *Lin28a* can confer the higher bioenergetic capacities needed to activate adult cells out of quiescence to enhance tissue repair.

DISCUSSION

Why some animals can fully regenerate organs when others cannot is a longstanding mystery of biology. Recent reports have shown that neonatal mice and select mouse strains have underappreciated regenerative capabilities, suggesting that some of the evolutionary ability to regenerate is retained in mammals but lost with development and age (Porrello et al., 2011; Clark et al., 1998). Most *in vivo* experiments have focused on loss of function screens in highly regenerative organisms like zebrafish and planaria. We have taken an alternative approach to this question by engineering improved tissue repair in mice, then discerning the underlying mechanisms.

Our work demonstrates that the highly conserved heterochronic gene and juvenility regulator *Lin28a*, first described in a genetic screen for *C. elegans* mutants with altered developmental timing (Ambros and Horvitz, 1984), promotes mammalian tissue repair by altering cellular metabolism. *Lin28a* is highly expressed in the early mammalian embryo, declines during mid-gestation, and silenced in most tissues after birth (Shyh-Chang and Daley, 2013). We have shown that engineering *Lin28a* reactivation in post-natal tissues reactivates an embryonic metabolic state that confers a reparative potential reminiscent of embryonic tissues. More generally, our studies support the concept that mammalian tissue repair can be substantially improved by engineering the reactivation of genes that regulate juvenile developmental stages. Importantly however, some tissues such as adult digits and the adult heart do not show improved tissue repair (Fig. S2, S7), illustrating that *Lin28a's* influence is context dependent. In the zebrafish, *lin-28* reactivation has also been found to promote retinal regeneration (Ramachandran et al., 2010).

It is surprising that *Lin28a* can promote tissue repair through mechanisms independent of *let-7*. Although overexpression of *let-7* could inhibit tissue repair, *let-7* repression alone failed to promote it. Though *let-7* repression is necessary but insufficient to promote tissue repair, it is possible that *let-7*-dependent and independent functions of *Lin28* synergize during tissue repair. There is ample evidence that *Lin28a*, like other RNA-binding proteins, regulates the translation of thousands of mRNAs and thus operates at the systems level (Peng et al., 2011; Wilbert et al., 2012; Cho et al., 2012). Future mechanistic and therapeutic investigation will focus on identifying additional targets of *Lin28a* that might also play a role in tissue repair.

Lin28a is emerging as a progenitor and stem cell factor that regulates metabolism to promote self-renewal (Shyh-Chang et al., 2013b), and here we demonstrate its effects in

vivo. Since specific inhibition of OxPhos can negate *Lin28a*'s beneficial effects on tissue repair without detriment to WT tissue repair, *Lin28a* is promoting tissue repair at least in part by enhancing oxidative metabolism and bioenergetics. Mechanistically, enhanced ATP/AMP and GTP/GMP ratios could supply the higher energetic needs of anabolic biosynthesis, mitosis, and migration during tissue repair, or promote growth signaling pathways like mTOR, all of which are enhanced by *Lin28a.* It is interesting to note that prior studies have linked the PPARs (peroxisome proliferator-activated receptors), master regulators of mitochondrial biogenesis and oxidative metabolism, to tissue repair in the mammalian skin, liver, muscles, and cornea (Michalik et al., 2001; Anderson et al., 2002; Angione et al., 2011; Nakamura et al., 2012). ATP-powered ion gradients and ROS have also been found to be critical in other regenerative animal models, such as *Xenopus* tail and planarian regeneration (Adams et al., 2007; Beane et al., 2011; Love et al., 2013). Clinically, the utility of topical oxygen for chronic wound therapy (Schreml et al., 2010), might also be partially related to the metabolic mechanisms that we have identified for *Lin28a*. Our findings support the novel use for *Lin28a* and the enhancement of oxidative metabolism for treating injuries and diseases resulting from tissue damage and degeneration.

EXPERIMENTAL PROCEDURES

Mice

All animal procedures were based on animal care guidelines approved by the Institutional Animal Care and Use Committee.

Digit amputation

Neonatal mice were cryoanesthetized before the forelimb and hindlimb central digits 2, 3, and 4 were amputated at the distal interphalangeal joint using a #11 scalpel under a dissection microscope. In all animals, right limb digits were left un-amputated as controls. Digit regrowth was measured as % of the uninjured digit length. In adults, mice were anesthetized with ketamine/xylazine before 400μm of hindlimb digits 2 and 4 were amputated using a #11 scalpel. Digit 3 was left unamputated as a control. X-ray imaging was performed using the MX-20 Specimen Radiograph System (Faxitron, Tucson, AZ).

Ear hole punch assay

A 2-mm-diameter hole (large) was punched in the center of each outer ear (pinna) by using a clinical biopsy punch (Roboz, Gaithersburg, MD). For profiling experiments, the entire pinna was punched throughout with 1-mm-diameter holes (small) to maximize the amount of pinnal tissue undergoing tissue repair.

Quantitative RT-PCR, Western blot and Immunohistochemistry

All assessments of mRNA levels were performed by qRT-PCR using commercial primers (OriGene), and all assessments of protein levels were performed by Western immunoblotting with anti-Lin28a, anti-tubulin (Cell Signaling), anti-Ndufb8, anti-Pdha1, anti-Pfkp, anti-Sdha, (Abcam), anti-Idh3b, or anti-Ndufb3 (Santa Cruz). For immunohistochemistry, sections were incubated with anti-Lin28a (Cell Signaling), anti-Lin28b (Cell Signaling), anti-Ki-67 (Dako), anti-phospho-H3 (Ser10) or anti-BrdU (Cell Signaling), and visualized using the VECTASTAIN Elite ABC System (Vector Labs).

RNA immunoprecipitation

Cells and tissues were lysed in M2 buffer with RNAse inhibitor, then incubated with anti-FLAG M2 affinity gel beads (Sigma Aldrich) according to the manufacturer's instructions,

to pull-down FLAG-tagged Lin28a. After 4 washes with M2 buffer, RNA bound to the M2 affinity gel beads was isolated using Trizol (Invitrogen).

Metabolomics, and Seahorse Analyzer

Metabolomics analysis was performed as previously described (Shyh-Chang et al., 2013a). Seahorse data analysis was performed as previously described (Wu et al., 2007).

Drug treatments

For the pinnal repair experiments, 25uL of 5mM 2-deoxy-D-glucose, 100uM 3-bromopyruvate, 500nM antimycin-A, or 10mM N-acetyl-cysteine, was applied topically on each ear 3 times a week, with 1 g/L dox dissolved in DMSO as the vehicle control. LNA antimiRs (Exiqon, Denmark) were injected subcutaneously once weekly as previously described (Frost and Olson 2011), or applied topically with 25ug LNA per ear using jetPEI according to manufacturer instructions (Polyplus, France).

Histology

Tissue samples were fixed in 10% buffered formalin or Bouin's solution and embedded in paraffin.

Statistical analysis

Data is presented as mean ± SEM, and Student's t-test (two-tailed distribution, two-sample unequal variance) was used to calculate *p* values. Statistical significance is displayed as $p < 0.05$ (one asterisk) or $p < 0.01$ (two asterisks) unless specified otherwise. The tests were performed using Microsoft Excel.

Supplementary Material

Refer to Web version on PubMed Central for supplementary material.

Acknowledgments

We thank John Powers, Costas Lyssiotis, Charles Kaufman, Jessica Lehoczky, and Clifford Tabin for invaluable feedback and discussions, Jin Zhang and the lab of Marcia Haigis for help with the Seahorse Analyzer, Min Yuan and Susanne Breitkopf for help with metabolomics, Samar Shah and Akiko Yabuuchi for help with the mouse work, Asher Bomer for help with the scratch assays, James Thornton for help with Northern blots, Roderick Bronson and the Harvard Medical School Rodent Histopathology Core for mouse tissue pathology. This work was supported by an A*STAR National Science Scholarship to N.S.C., a Graduate Training in Cancer Research Grant, a American Cancer Society Postdoctoral Fellowship, an NIH K08 grant and a CPRIT award to H.Z., a Herchel Smith Graduate Fellowship to K.M.T., and a grant from the Ellison Medical Foundation to G.Q.D. G.Q.D. is an investigator of the Howard Hughes Medical Institute and the Manton Center for Orphan Disease Research.

References

Adams DS, et al. H+ pump-dependent changes in membrane voltage are an early mechanism necessary and sufficient to induce Xenopus tail regeneration. Development. 2007; 1335:1323–1335. [PubMed: 17329365]

Ambros V, Horvitz H. Heterochronic mutants of the nematode Caenorhabditis elegans. Science. 1984; 226:409–416. [PubMed: 6494891]

Anchelin M, et al. Behaviour of telomere and telomerase during aging and regeneration in zebrafish. PloS One. 2011; 6:e16955. [PubMed: 21347393]

Anderson SP, et al. Delayed liver regeneration in peroxisome proliferator-activated receptor-α-null mice. Hepatology. 2002; 36:544–54. [PubMed: 12198646]

Angione AR, et al. PPARδ regulates satellite cell proliferation and skeletal muscle regeneration. Skelet Muscle. 2011; 1:1–33. [PubMed: 21798079]

Beane WS, et al. A Chemical Genetics Approach Reveals H, K-ATPase-Mediated Membrane Voltage Is Required for Planarian Head Regeneration. Chem Biol. 2011; 18:77–89. [PubMed: 21276941]

Chadwick RB, et al. Digit tip regrowth and differential gene expression in MRL/Mpj, DBA/2, and C57BL/6 mice. Wound Repair Regen. 2007; 15:275–84. [PubMed: 17352761]

Cho J, et al. LIN28A Is a Suppressor of ER-Associated Translation in Embryonic Stem Cells. Cell. 2012; 151:765–77. [PubMed: 23102813]

Clark LD, et al. A new murine model for mammalian wound repair and regeneration. Clin Immunol Immunopathol. 1998; 88:35–45. [PubMed: 9683548]

Conboy IM, et al. Rejuvenation of aged progenitor cells by exposure to a young systemic environment. Nature. 2005; 433:760–4. [PubMed: 15716955]

Darwin C. The Variation of Animals and Plants Under Domestication. (Forgotten Books Classic Reprint Series). 1887

Deuchar BEM. Regeneration of amputated limb-buds in early rat embryos. J Embryol Exp Morphol. 1976; 35:345–354. [PubMed: 939943]

Frost RJA, Olson EN. Control of glucose homeostasis and insulin sensitivity by the Let-7 family of miRNAs. Proc Natl Acad Sci USA. 2011; 108:21075–80. [PubMed: 22160727]

Goss RJ, Grimes LN. Epidermal downgrowths in regenerating rabbit ear holes. J Morphol. 1975; 146:533–42. [PubMed: 1171254]

Gourevitch DL, et al. Dynamic changes after murine digit amputation: the MRL mouse digit shows waves of tissue remodeling, growth, and apoptosis. Wound Repair Regen. 2009; 17:447–55. [PubMed: 19660054]

Guo S, DiPietro LA. Factors Affecting Wound Healing. J Dent Res. 2010; 89:219–229. [PubMed: 20139336]

Heo I, et al. Lin28 mediates the terminal uridylation of let-7 precursor MiRNA. Mol Cell. 2008; 32:276–84. [PubMed: 18951094]

Kaplon J, et al. A key role for mitochondrial gatekeeper pyruvate dehydrogenase in oncogene-induced senescence. Nature. 2013; 498:109–112. [PubMed: 23685455]

Leinonen JT, et al. Association of LIN28B with Adult Adiposity-Related Traits in Females. PloS One. 2012; 7:e48785. [PubMed: 23152804]

Lettre G, et al. Identification of ten loci associated with height highlights new biological pathways in human growth. Nat Genet. 2008; 40:584–91. [PubMed: 18391950]

Liu J, et al. Regenerative phenotype in mice with a point mutation in transforming growth factor β type I receptor (TGFBR1). Proc Natl Acad Sci USA. 2011; 108:14560–5. [PubMed: 21841138]

Love NR, et al. Amputation-induced reactive oxygen species are required for successful Xenopus tadpole tail regeneration. Nat Cell Biol. 2013; 15:222–8. [PubMed: 23314862]

Michalik L, et al. Impaired skin wound healing in peroxisome proliferator receptor (PPAR)α and PPARβ mutant mice. J Cell Biol. 2001; 154:799–814. [PubMed: 11514592]

Miyauchi H, et al. Akt negatively regulates the in vitro lifespan of human endothelial cells via a p53/p21-dependent pathway. EMBO J. 2004; 23:212–20. [PubMed: 14713953]

McBrearty BA, et al. Genetic analysis of a mammalian wound-healing trait. Proc Natl Acad Sci USA. 1998; 95:11792–7. [PubMed: 9751744]

Moss EG, et al. The cold shock domain protein LIN-28 controls developmental timing in C. elegans and is regulated by the lin-4 RNA. Cell. 1997; 88:637–46. [PubMed: 9054503]

Muller-Rover S, et al. A Comprehensive Guide for the Accurate Classification of Murine Hair Follicles in Distinct Hair Cycle Stages. J Invest Dermatol. 2001; 117:3–15. [PubMed: 11442744]

Nakamura Y, et al. Functional role of PPARδ in corneal epithelial wound healing. Am J Pathol. 2012; 180:583–598. [PubMed: 22119718]

Newman M, et al. Lin-28 interaction with the Let-7 precursor loop mediates regulated miRNA processing. RNA. 2008; 14:1539–49. [PubMed: 18566191]

Nishino J, et al. Hmga2 promotes neural stem cell self-renewal in young but not old mice by reducing p16Ink4a and p19Arf Expression. Cell. 2008; 135:227–39. [PubMed: 18957199]

Nogueira V, et al. Akt determines replicative senescence and oxidative or oncogenic premature senescence and sensitizes cells to oxidative apoptosis. Cancer Cell. 2008; 14:458–70. [PubMed: 19061837]

Ong KK, et al. Genetic variation in LIN28B is associated with the timing of puberty. Nat Genet. 2009; 41:729–33. [PubMed: 19448623]

Ong KK, et al. Associations between the pubertal timing-related variant in LIN28B and BMI vary across the life course. J Clin Endocrinol Metab. 2011; 96:E125–9. [PubMed: 20962026]

Pearson RD. Neotenic blastemal morphogenesis. Acta Biotheoretica. 1984; 33:51–59.

Peng S, et al. Genome-wide Studies Reveal that Lin28 Enhances the Translation of Genes Important for Growth and Survival of Human Embryonic Stem Cells. Stem Cells. 2011; 29:496–504. [PubMed: 21425412]

Perry JRB, et al. Meta-analysis of genome-wide association data identifies two loci influencing age at menarche. Nat Genet. 2009; 41:648–50. [PubMed: 19448620]

Polesskaya A, et al. Lin-28 binds IGF-2 mRNA and participates in skeletal myogenesis by increasing translation efficiency. Genes Dev. 2007; 21:1125–38. [PubMed: 17473174]

Porrello ER, et al. Transient Regenerative Potential of the Neonatal Mouse Heart. Science. 2011; 331:1078–1080. [PubMed: 21350179]

Poss KD. Advances in understanding tissue regenerative capacity and mechanisms in animals. Nat Rev Genet. 2010; 11:710–721. [PubMed: 20838411]

Ramachandran R, et al. Ascl1a regulates Muller glia dedifferentiation and retinal regeneration through a Lin-28-dependent, let-7 microRNA signalling pathway. Nat Cell Biol. 2010; 12:1101–7. [PubMed: 20935637]

Rybak A, et al. A feedback loop comprising lin-28 and let-7 controls pre-let-7 maturation during neural stem-cell commitment. Nat Cell Biol. 2008; 10:987–93. [PubMed: 18604195]

Sanchez Alvarado A, Tsonis PA. Bridging the regeneration gap: genetic insights from diverse animal models. Nat Rev Genet. 2006; 7:873–84. [PubMed: 17047686]

Schreml S, et al. Oxygen in acute and chronic wound healing. Br J Dermatol. 2010; 163:257–68. [PubMed: 20394633]

Shah MV, et al. The role of canonical Wnt signaling in leg regeneration and metamorphosis in the red flour beetle Tribolium castaneum. Mech Dev. 2011; 128:342–58. [PubMed: 21801833]

Shinoda G, et al. Fetal deficiency of Lin28 programs life-long aberrations in growth and glucose metabolism. Stem Cells. 2013 Epub ahead of print. 10.1002/stem.1423

Shyh-Chang N, et al. Influence of threonine metabolism on S-adenosylmethionine and histone methylation. Science. 2013a; 339:222–6. [PubMed: 23118012]

Shyh-Chang N, et al. Stem cell metabolism in tissue development and aging. Development. 2013b; 140:2535–47. [PubMed: 23715547]

Shyh-Chang N, Daley GQ. Lin28: primal regulator of growth and metabolism in stem cells. Cell Stem Cell. 2013; 12:395–406. [PubMed: 23561442]

Smith-Bolton RK, et al. Regenerative Growth in Drosophila Imaginal Discs Is Regulated by Wingless and Myc. Dev Cell. 2009; 16:797–809. [PubMed: 19531351]

Sulem P, et al. Genome-wide association study identifies sequence variants on 6q21 associated with age at menarche. Nat Genet. 2009; 41:734–8. [PubMed: 19448622]

Viswanathan SR, et al. Selective blockade of miRNA processing by Lin28. Science. 2008; 320:97–100. [PubMed: 18292307]

Widén E, et al. Distinct variants at LIN28B influence growth in height from birth to adulthood. Am J Hum Genet. 2010; 86:773–82. [PubMed: 20398887]

Wilbert ML, et al. LIN28 Binds Messenger RNAs at GGAGA Motifs and Regulates Splicing Factor Abundance. Mol Cell. 2012; 48:195–206. [PubMed: 22959275]

Wu M, et al. Multiparameter metabolic analysis reveals a close link between attenuated mitochondrial bioenergetic function and enhanced glycolysis dependency in human tumor cells. Am J Physiol Cell Physiol. 2007; 292:C125–36. [PubMed: 16971499]

Yang D, Moss E. Temporally regulated expression of Lin-28 in diverse tissues of the developing mouse. Gene Expr Patterns. 2003; 3:719–726. [PubMed: 14643679]

Yokoyama S, et al. Dynamic gene expression of Lin-28 during embryonic development in mouse and chicken. Gene Expr Patterns. 2008; 8:155–60. [PubMed: 18077221]

Young HE, et al. Gross morphological analysis of limb regeneration in postmetamorphic adult Ambystoma. Anat Rec. 1983; 206:295–306. [PubMed: 6614512]

Zhu H, et al. Lin28a transgenic mice manifest size and puberty phenotypes identified in human genetic association studies. Nat Genet. 2010; 42:9–11.

Zhu H, et al. The Lin28/let-7 axis regulates glucose metabolism. Cell. 2011; 147:81–94. [PubMed: 21962509]

HIGHLIGHTS

1. *Lin28a* reactivation promotes hair regrowth, as well as ear and digit tissue repair.
2. Excess *let-7* inhibits tissue repair, but anti-*let-7* therapy fails to promote tissue repair.
3. *Lin28a* promotes tissue repair by enhancing the translation of some oxidative enzymes.
4. *Lin28a*'s enhancement of tissue repair was negated by OxPhos inhibition.

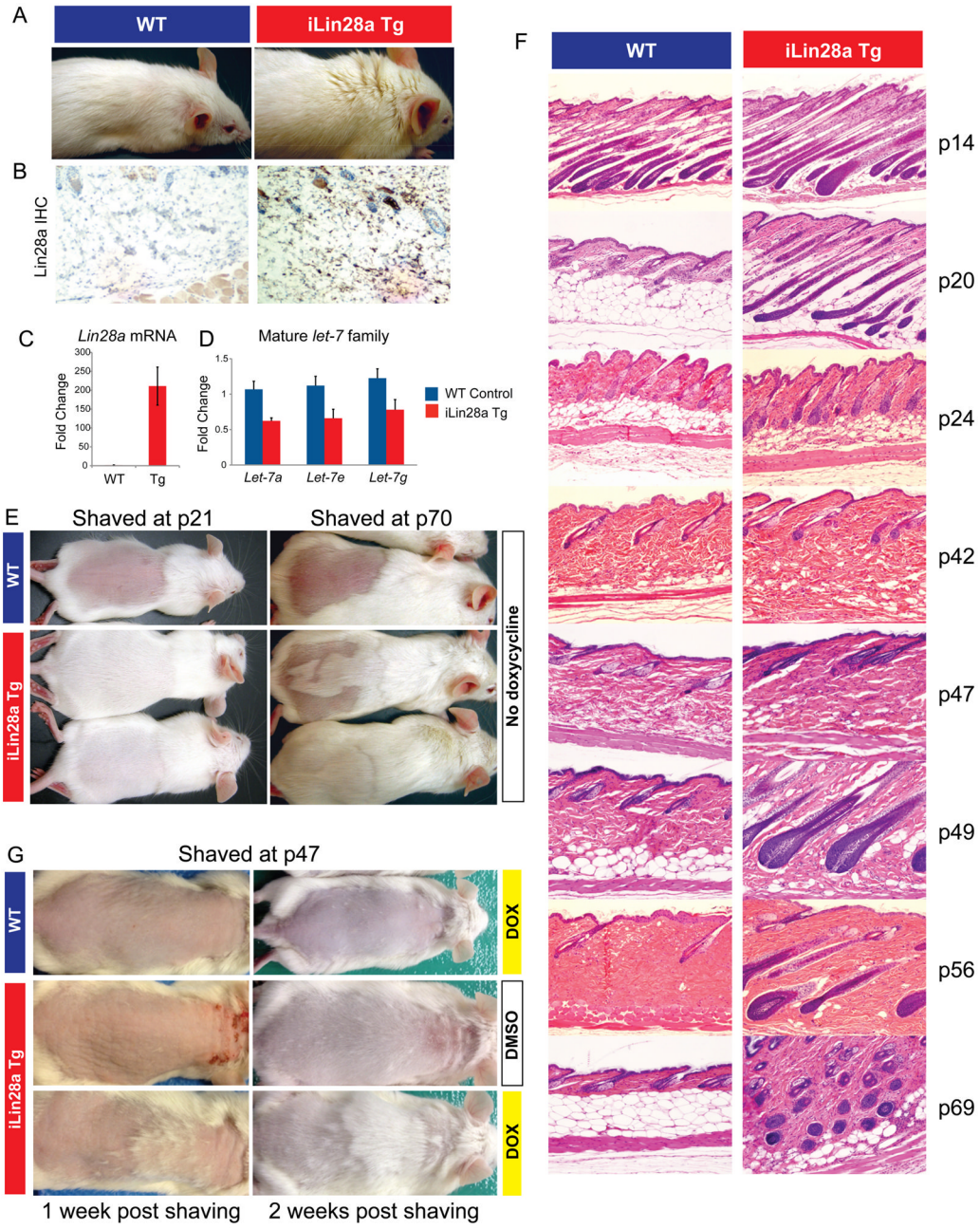

Figure 1. Lin28a reactivation promotes hair regrowth

A. Uninduced iLin28a Tg mice possess a thicker fur coat than WT mice.

B. *Lin28a* expression in the skin of WT or iLin28a Tg mice as determined by immunohistochemistry.

C. *Lin28a* mRNA levels as determined by qRT-PCR.

D. Mature *let-7* expression as determined by qRT-PCR in tail epidermis of WT and uninduced iLin28a Tg mice.

E. Hair regrowth in mice shaved at p21 was observed 1 week post-shaving in 0/6 WT vs. 6/6 Lin28a Tg littermates (Left image). Hair regrowth in mice shaved at p70 was observed 3 weeks post-shaving in 0/6 WT vs. 5/5 iLin28a Tg littermates (Right image).

F. Histologic hair cycle analysis over 10 weeks. All sections are 10x and H+E stained.

G. Hair regrowth on dorsal skin in topical dox-treated p47 WT and iLin28a Tg littermates, 1 and 2 weeks after shaving. Ectopic hair regrowth was observed in 0/4 WT dox treated vs. 0/3 DMSO treated Tg vs. 3/4 dox induced Tg mice. Data are represented as mean +/− SEM, * $P<0.05$, ** $P< 0.01$. See also Figure S1.

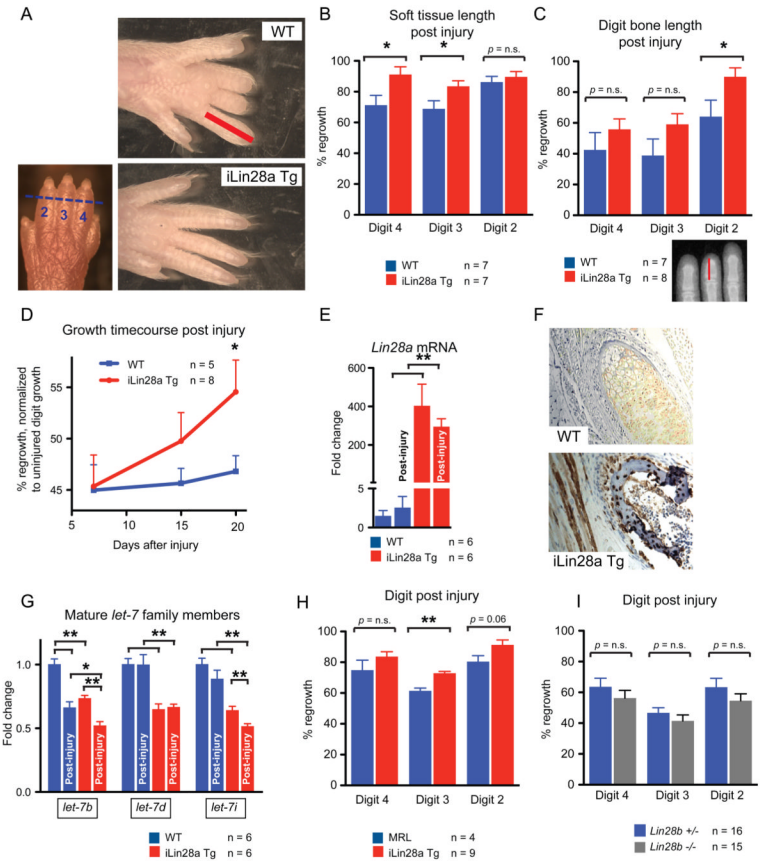

Figure 2. *Lin28a* reactivation promotes regrowth of digits after neonatal amputation

For all digit measurements, % regrowth is quantified by dividing the length of the regrowing digit in the injured limb with the length of the normal digit on the opposite uninjured limb.

A. Left image shows p1 digits and the amputation site (blue hash mark). Right images show digits 21 days after neonatal digit amputation. Red bar depicts the soft tissue dimension measured between the digit tip and the proximal interphalangeal joint.

B. Quantification of soft tissue regrowth 21 days after neonatal digit amputation.

C. Quantification of bone regrowth 21 days after neonatal digit amputation. X-ray film with red bar showing that bone length was measured from the proximal interphalangeal joint.

D. Post-injury growth kinetics (as % of uninjured digit length) over 21 days.

E. *Lin28a* mRNA expression in WT, injured WT, iLin28a Tg, and injured iLin28a Tg digits, as determined by qRT-PCR.

F. Immunohistochemistry indicating Lin28a protein expression in Tg and WT bone from the neonatal skeleton.

G. Mature *let-7* expression in WT, injured WT, iLin28a Tg, and injured iLin28a Tg digits, as determined by qRT-PCR.

H. Digit tip regrowth in iLin28a Tg mice backcrossed onto the hyper-regenerative MRL strain background. Control mice are WT MRL littermates. Data are represented as mean +/− SEM, * P<0.05, ** P< 0.01. See also Figure S2.

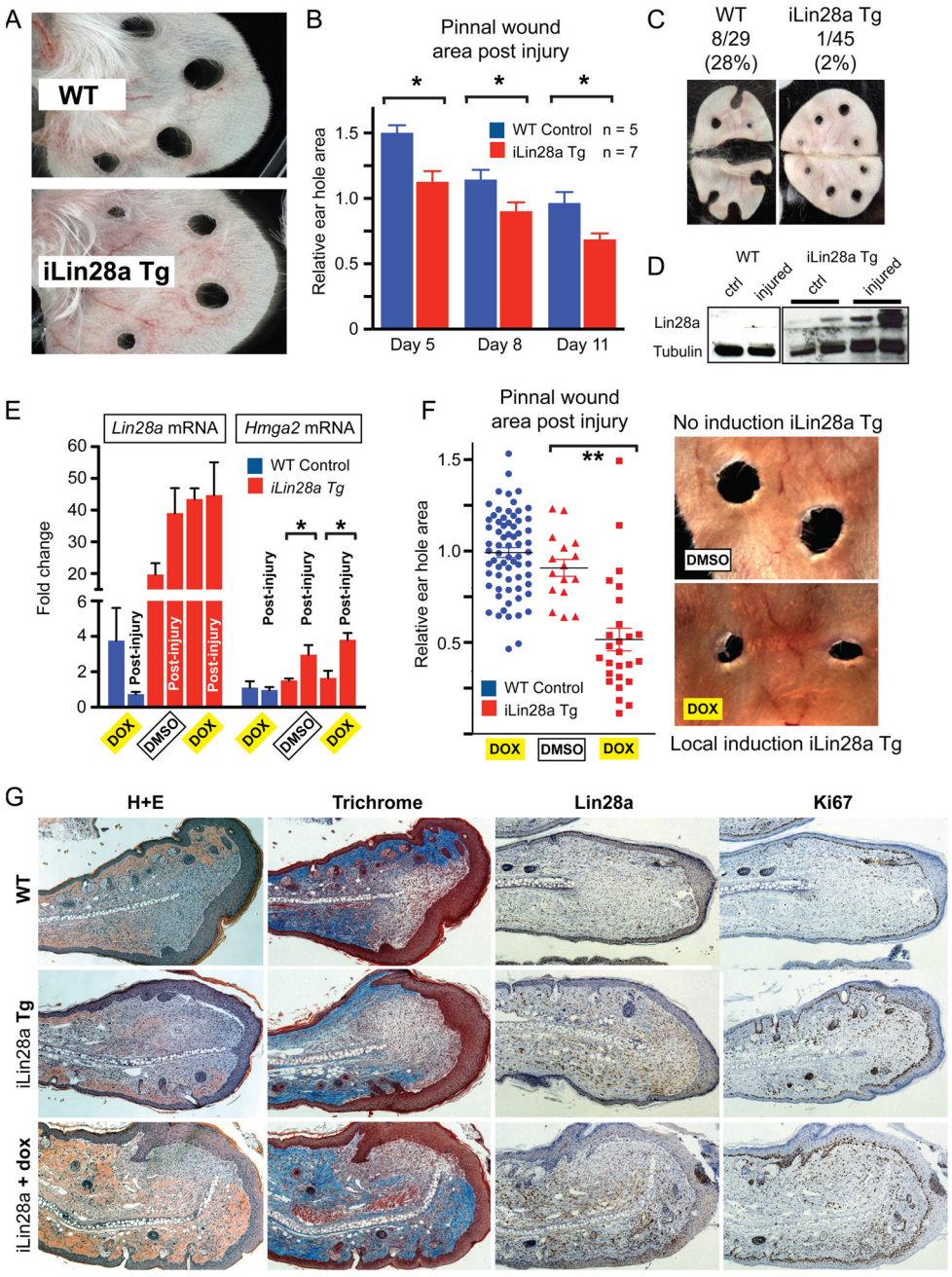

Figure 3. *Lin28a* reactivation promotes pinnal tissue repair

A. WT and iLin28a Tg wound healing 8 days after 2mm-diameter ear hole punches.

B. Wound area size at day 5, 8, and 11, during the course of wound healing.

C. Proportion of WT and iLin28a Tg ear holes torn by mice after ear hole punching.

D. Western blot indicating Lin28a protein levels in topical dox-treated iLin28a Tg ears, before (n=2) and 3 days after (n=2) injury, compared to WT ears.

E. mRNA levels of *Lin28a* and the *let-7* target *Hmga2* in topical dox-treated iLin28a Tg ears, as determined by qRT-PCR.

F. Wound area size after 10 days of local topical treatment with dox.

G. H+E, trichrome, Lin28a, and Ki-67 staining in WT, iLin28a Tg and induced iLin28a Tg mice. Data are represented as mean +/− SEM, * P<0.05, ** P< 0.01. See also Figure S3.

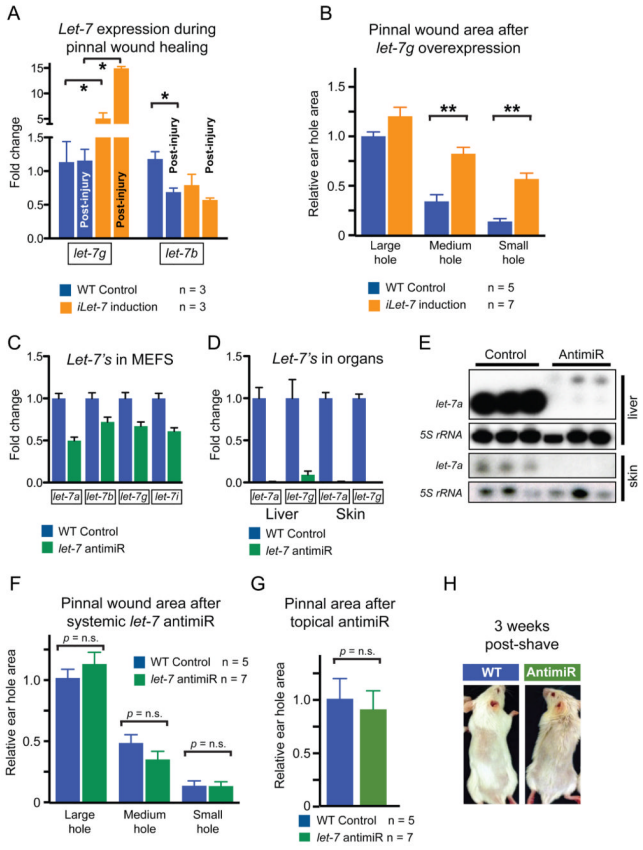

Figure 4. *Let-7* repression is necessary but insufficient for tissue repair

A. Expression of mature *let-7g* and *let-7b* in WT and iLet-7 ears, before and after injury, as determined by qRT-PCR.

B. Ear hole wound area size after whole animal *let-7g* induction in iLet-7 mice.

C. Mature *let-7* miRNA expression in MEFs after *let-7* antimiR treatment, as determined by qRT-PCR.

D. Mature *let-7* miRNA expression in vivo after 2 subcutaneous injections of *let-7* antimiR.

E. Northern blot indicating *let-7a* levels in the liver and skin of control and *let-7* antimiR-treated WT mice.

F. Ear hole wound size after subcutaneous *let-7* antimiR treatment of WT mice.

G. Ear hole wound size after local topical *let-7* antimiR treatment of WT mice.

H. Hair regrowth after *let-7* antimiR treatment of WT mice. Data are represented as mean +/− SEM, * P<0.05, ** P< 0.01.

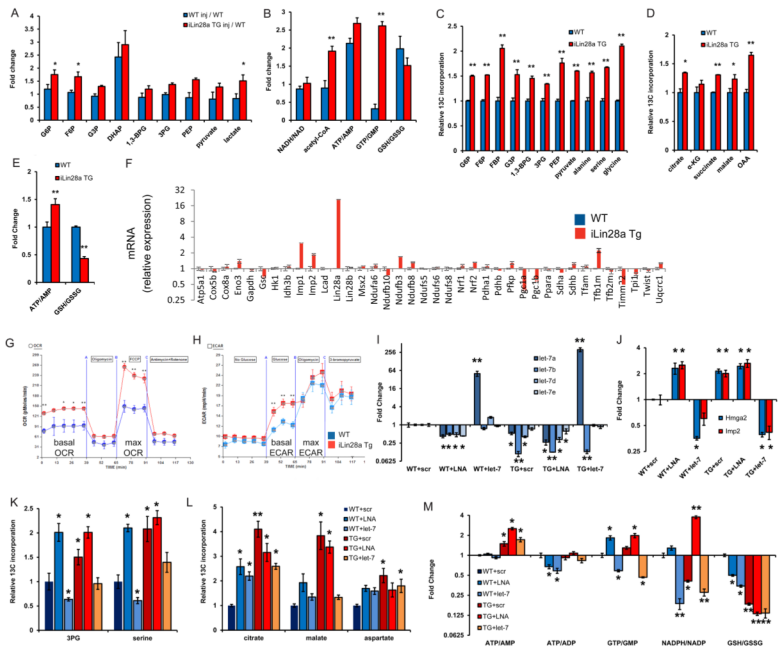

Figure 5. *Lin28a* alters the bioenergetic state during tissue repair

A. LC-MS/MS selected reaction monitoring (SRM) analysis of abundance in glycolysis intermediates in WT and iLin28a Tg pinnal tissue after injury (inj), relative to WT uninjured pinnae. G3P, D-glyceraldehyde-3-phosphate. DHAP, dihydroxyacetone-phosphate. BPG, 1,3-bisphosphoglycerate. 3PG, 3-phosphoglycerate. PEP, phosphoenolpyruvate.

B. SRM analysis of several metabolic indicators in WT and iLin28a Tg pinnal tissue after injury (inj), relative to WT uninjured pinnae. ATP, adenosine-5′-triphosphate. AMP, adenosine-5′-monophosphate. GTP, guanosine-5′-triphosphate. GMP, guanosine-5′-monophosphate. GSH/GSSG, glutathione/glutathione disulfide.

C. Fraction of glycolytic intermediates labeled by ^{13}C, derived from [U-^{13}C]glucose in MEFs over 30 minutes, as measured by SRM analysis (n=3).

D. Fraction of Krebs cycle intermediates labeled at 2 carbons by ^{13}C, derived from [U-^{13}C]glucose in MEFs over 8 hours, as measured by SRM analysis (n=3).

E. SRM analysis of the ATP/AMP and GSH/GSSG ratios in WT and iLin28a Tg MEFs (n=3).

F. Mitochondrial biogenesis, glycolytic enzyme, and *let-7* target mRNAs, analyzed by qRT-PCR. *Lin28a*, and the *let-7* targets *Imp1* and *Imp2* served as positive controls. Relative expression levels were normalized to WT MEFs.

G. Oxygen consumption rate (OCR) of WT and iLin28a Tg MEFs, as measured by the Seahorse Analyzer (n=4 each). Oligomycin treatment inhibits ATP synthase-dependent OCR, the proton gradient uncoupler FCCP then induces maximal OCR, and antimycin/rotenone finally inhibits all OxPhos-dependent OCR.

H. Extracellular acidification rate (ECAR) of WT and iLin28a Tg MEFs, as measured by the Seahorse Analyzer (n=4 each). Addition of glucose induces glycolysis-dependent lactic acid production and ECAR, oligomycin then induces maximal ECAR, and 3BP partially inhibits glycolysis-dependent ECAR.

I. Mature *let-7* expression in WT and iLin28a Tg MEFs, after transfection with a scrambled (scr) control, *let-7* LNA antimiR, or *let-7a* duplex, as determined by qRT-PCR.

J. Expression of the *let-7* targets *Hmga2* and *Imp2* in WT and iLin28a Tg MEFs, after transfection with a scrambled (scr) control, *let-7* LNA antimiR, or *let-7a* duplex, as determined by qRT-PCR.

K. Fraction of the glycolytic intermediate 3-phosphoglycerate (3PG) and the glycolytic side-product serine, labeled by ^{13}C derived from [U-^{13}C]glucose over 30 minutes, in MEFs after transfection with a scrambled (scr) control, *let-7* LNA antimiR, or *let*-7*a* duplex (n=3).
L. Fraction of the Krebs cycle intermediates citrate, malate and oxaloacetate-derived aspartate, labeled at 2 carbons by ^{13}C derived from [U-^{13}C]glucose over 8 hours, in MEFs after transfection with a scrambled (scr) control, *let-7* LNA antimiR, or *let*-7*a* duplex (n=3).
M. SRM analysis of several metabolic indicators in WT and iLin28a Tg MEFs after transfection with a scrambled (scr) control, *let-7* LNA antimiR, or *let*-7*a* duplex (n=3). Data are represented as mean +/− SEM, * $P<0.05$, ** $P< 0.01$. See also Figure S5.

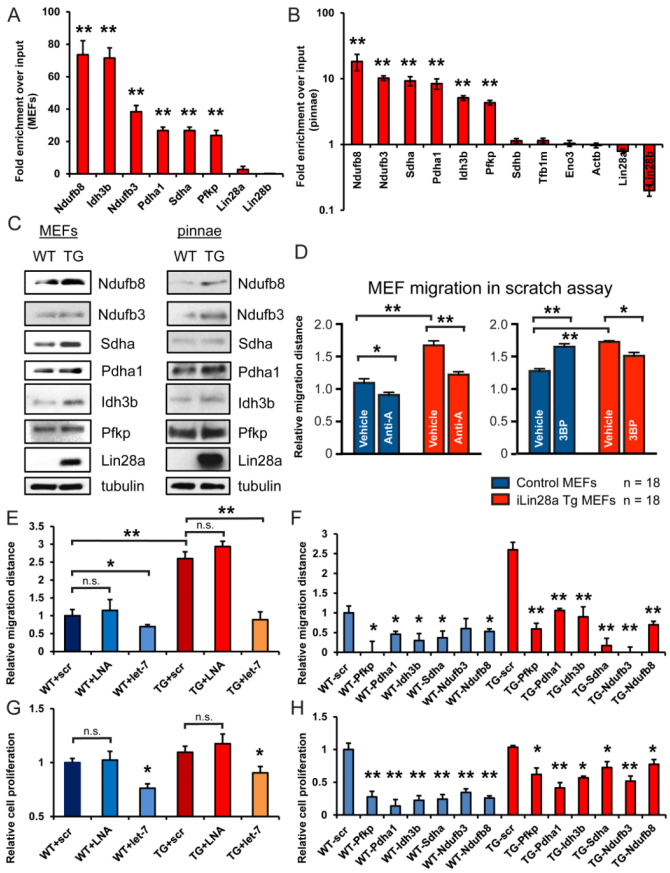

Figure 6. *Lin28* promotes wound healing in vitro by enhancing bioenergetic metabolism

A. RNA immunoprecipitation (RIP) using FLAG-tagged Lin28a and subsequent RT-PCR shows the metabolic enzyme mRNAs bound by Lin28a in MEFs in vitro.

B. RNA immunoprecipitation (RIP) using FLAG-tagged Lin28a and subsequent RT-PCR shows the metabolic enzyme mRNAs bound by Lin28a in pinnal tissues in vivo.

C. Western blots for Lin28a mRNA targets in primary MEFs and pinnal tissues in vivo,

D. Distance traveled by WT and iLin28a Tg MEFs, 18 hours after a defined scratch was made on equal-numbered monolayers (n=18). MEFs were treated with 50nM Anti-A, 100uM 3BP, or DMSO vehicle control immediately after the scratch.

E. Distance traveled by WT and iLin28a Tg MEFs treated with a scrambled (scr) control, *let-7* LNA antimiR, or *let-7a* duplex.

F. Distance traveled by WT and iLin28a Tg MEFs treated with siRNAs against metabolic enzymes.

G. Cell proliferation of WT and iLin28a Tg MEFs treated with a scrambled (scr) control, *let-7* LNA antimiR, or *let-7a* duplex.

H. Cell proliferation of WT and iLin28a Tg MEFs treated with siRNAs against metabolic enzymes. Data are represented as mean +/− SEM, * P<0.05, ** P< 0.01. See also Figure S6.

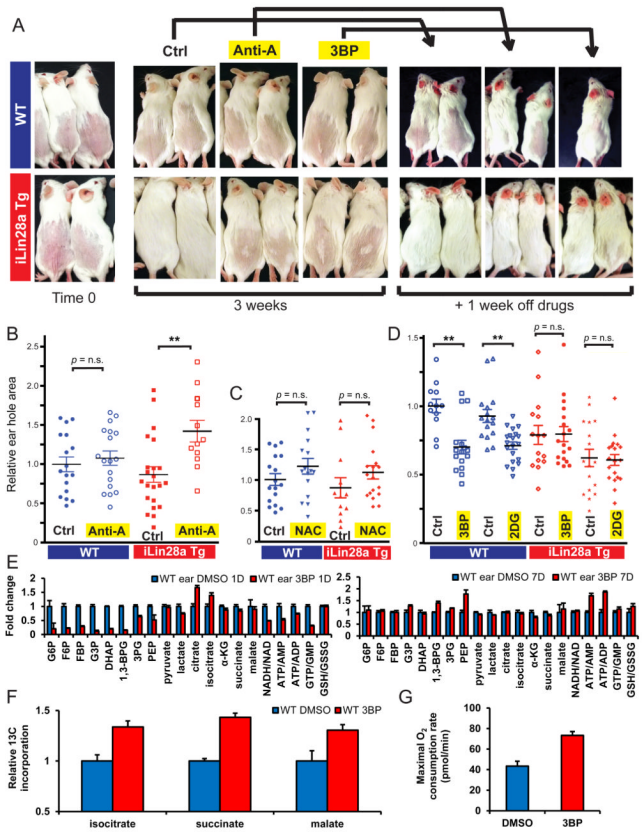

Figure 7. *Lin28* promotes tissue repair in vivo by enhancing bioenergetic metabolism

A. Hair regrowth of dorsal skin in p42 iLin28a Tg mice and WT littermates, at the time of shaving, and 3 weeks after local topical treatment with 3BP, or Anti-A, dissolved in 1g/L dox in DMSO (Ctrl). Mice were then taken off all treatment for 1 week.

B. Pinnal wound size after 10 days of local topical treatment with Anti-A, dissolved in 1g/L dox in DMSO (Ctrl), on both iLin28a Tg and WT littermate ear holes.

C. Pinnal wound size after 10 days of local topical treatment with the antioxidant N-acetyl-cysteine (NAC) dissolved in 1g/L dox in DMSO (Ctrl), on both iLin28a Tg and WT littermate ear holes.

D. Pinnal wound size after 10 days of local topical treatment with the glycolysis inhibitors 3BP or 2-deoxy-D-glucose (2DG) dissolved in 1g/L dox in DMSO (Ctrl), on both iLin28a Tg and WT littermate ear holes.

E. Metabolomic profiling on WT ears 1 and 7 days after daily 3BP treatment. Shown are glycolytic intermediates and the bioenergetics ratios NADH/NAD, ATP/AMP, ATP/ADP, and GTP/GMP (n=4).

F. Fraction of the Krebs cycle intermediates isocitrate, succinate, and malate, labeled at 2 carbons by ^{13}C derived from [U-^{13}C]glucose over 8 hours, in WT MEFs after continuous incubation in 3BP for 3 days (n=3).

G. Maximal O_2 consumption rate in WT MEFs after continuous incubation in 3BP for 3 days (n=6). Data are represented as mean +/− SEM, * P<0.05, ** P< 0.01.